Circular Concentric-Ring Reflectarray Design Using a Coaxial Wedge Unit Cell

Joshua S. Roper and Andrew F. Peterson

School of Electrical and Computer Engineering
Georgia Institute of Technology, Atlanta, GA 30332, USA
jroper33@gatech.edu, afpeterson@gatech.edu

Abstract ─ This paper presents a design methodology for a concentric ring reflectarray using angular periodic structures. This paper also examines the coaxial wedge unit cell using the waveguide simulator method and contrasts it to the coaxial unit ring approach. The coaxial wedge unit cell approach is seen to offer a more efficient and more extendable means of simulation than the coaxial unit ring approach.

Index Terms ─ Coaxial waveguide, frequency selective surface, periodic structures, reflectarray, waveguide, waveguide simulator method.

I. INTRODUCTION

The reflectarray, an antenna concept that combines design and analysis techniques from reflector antennas, periodic microwave structures and antenna array theory, has been around since at least the 1960s [1]. Early research was focused on waveguide elements. Planar elements such as spirals, discs, and patches were explored in the 1970s [2-4]. The first reflectarray patent was filed in the 1980s [5]. This early research was mainly conducted by private companies and the U.S. Air Force for military applications.

In the 1990s microstrip reflectarray design concentrated on analyzing the phase behavior as a function of patch size through full wave analysis [6-9]. Essential reflectarray capacities were also investigated including: beamsteering [10], multiple polarizations [11], bandwidth improvement [12], and dual-frequency band operation [13]. Recent advancements have been focused on improving upon these capabilities and enhancing performance metrics.

The reflectarray is a flat surface supporting many elements (usually microstrip patches) that are not connected with power division lines. This antenna has the benefit of being high gain and high efficiency like the reflector antenna or antenna array, while being flat (unlike the reflector) and not having an expensive, high-loss beamformer (unlike the antenna array). Additionally, low-loss phase shifters can be incorporated to add an electronic beam steering capability (like the antenna array) [14-15]. The reflectarray can also be used as a subreflector, instead of a solid subreflector [16].

The reflectarray will usually have non-uniformly sized elements to produce a non-constant reflected phase. At a basic level, the design must provide a phase shift at each element such that the phase delay at that element will produce a uniform reflected phase after path length delay effects are taken into account. A plot of the phase delay or phase shift for a normal angle of incidence will show a series of peaks and nulls around the center of the reflectarray.

One way to produce the phase delay that is needed is to alter the element size as a function of distance from the center of the array. To design a reflectarray of this type, full wave simulations of many element sizes are conducted and then the resulting resonant frequencies are mapped into a "backwards-S" phase reflection curve. This curve is used to fit the required phase delay for the reflectarray. A detailed design overview is presented in the literature [17-18].

Initial work on simulating periodic structures began in the 1960s using the waveguide simulator (WGS) method [19]. This method relied on exciting a radiating element in a waveguide. Because of the surrounding perfect electric conductor (PEC) walls, a method of images environment is formed which extends the element into an infinite array.

The WGS method can be applied to any arbitrary shaped waveguide. In the following, the well-known cylindrical waveguide is used [20-21]. The waveguide simulator method was not applied to simulating structures of this sort until recently [22-24].

It is important to point out that advances have come for planar periodic structure simulation using Floquet conditions to account for the linear phase shifting along the elements in an infinite environment [25]. This approach is a staple of modern array simulations, but assumes a linear phase shifting of the frequency. Due to this fact, for curved or cylindrical designs where the phase shifting is not linear, the Floquet condition cannot be used and other methods must be explored.

Another design consideration is the reflectarray

Submitted On: June 24, 2018
Accepted On: October 13, 2018

feed. Feed design uses efficiency plots and the chosen focal-to-diameter (F/D) ratio of the array. A detailed design overview can be found from classical reflector antenna theory [26-27].

Once the phase behavior of the reflectarray element is determined and the feed designed, the far field characteristics of the antenna can be approximated using array theory. An array geometry of particular interest is the concentric ring array geometry as it has circular periodicity. This array has the drawback of relatively high sidelobes in the uniform case; therefore an amplitude taper or some optimization procedure must be employed. Reference [28] presents techniques to mitigate the sidelobes by as much as 10dB. An actual design would need to employ these techniques as the uniform case would violate FCC 25.209 regulations for Ku-band.

Other approaches and applications to this problem have been considered. A locally planar unit cell analysis can be conducted to get the reflectance and transmittance parameters and then these can be placed on the surface of a reflector for a diffraction analysis [29]. The square geometry of a patch can be warped into a quasi-trapezoidal shape and analyzed [30-31]. Planar results can be simulated for a rectangular patch and then rotated tangentially around a curved surface using the characteristic basis method and spectral rotation approach [32-33].

II. MODEL SETUP

A. Design geometry

In this work, the WGS method is used with Ansys HFSS to analyze angular planar periodic unit cells. A resonant frequency of 6.15GHz (C-Band Uplink) is chosen for this application. In satellite communications, C-Band typically uses circular polarization. Furthermore, C-Band involves a lower frequency than Ka or Ku-Bands and therefore imposes an easier simulation. A copper clad dielectric substrate of Rogers RO3003 with a standard thickness of 1.52mm is used as the medium of design.

The same geometry is used for both the unit ring and the unit cell, with the unit cell stacking rotationally about the center of the coax to form the unit ring. As an example, the angular width of the unit cell is set to 36° in order to make a full 360° unit ring with ten unit cells. The angular width of the patch is set to 24°. The inner and outer spacing above and below the patch is set to 5.9mm. The total length of the design is 0.43 wavelengths. The geometries of the unit cell and unit ring can be seen in Fig. 1.

The geometry is configured with a PEC back plate and is topped with a vacuum layer with a height of 2 wavelengths. The top of the vacuum is set to be a modally driven port, making this design a one-port device. It can be found analytically or via HFSS that the coaxial unit ring has 9 propagating modes and the unit cell has 1. To determine the number of propagating modes in HFSS the user must set the maximum number of allowable modes, run a few passes of the adaptive mesh, and then inspect the propagation constants (gamma) to see which modes have positive real (lambda) and imaginary (epsilon) values.

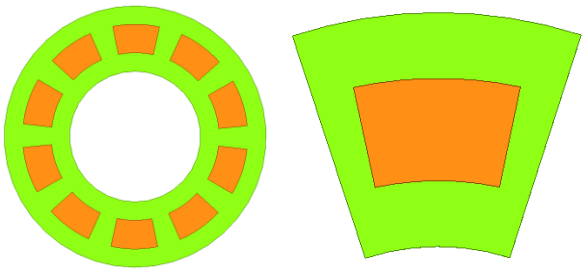

Fig. 1. (Left) Coaxial unit ring; (Right) coaxial wedge unit cell.

B. Boundary conditions

The boundary conditions for this design are depicted in Fig. 2. For the coaxial unit ring, the inner and outer coaxial walls are set to perfect magnetic conducting (PMC) boundary conditions to produce angularly polarized fields, as desired for this illustration. This type of polarization approximates illumination by a circularly polarized source. The boundaries can be also set to perfect electric conducting (PEC) boundary conditions to yield radially polarized fields (not depicted).

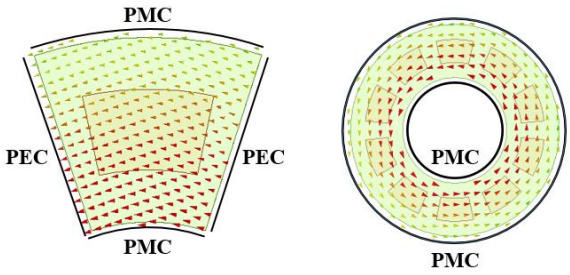

Fig. 2. (Left) Principal propagating mode on a coaxial unit cell; (Right) principal propagating mode on a coaxial wedge unit ring.

The coaxial unit cell (also depicted in Fig. 2) has the PMC boundary condition as well on the radial walls. Additionally, PEC boundary conditions are added to the side walls as a primitive periodic boundary condition. This can be thought about intuitively in two ways: 1) this will create images on these side walls to artificially extend the cell; 2) having the PEC on both side walls will make the fields want to jump from one to the other, creating the same fields in the cell as can be seen in the unit ring.

C. Meshing convergence

The coaxial wedge unit cell has only one propagating mode, and thus the mesh convergence optimization scheme is simple. This simulation is run as a modal solution of a one port cavity in the HFSS software, so the mesh refinement process is based on a single S-Parameter value S11 (magnitude and phase). For accuracy, the mesh is considered to have converged when there is a maximum change of no greater than 0.001 for the magnitude and 1 degree for the phase of S_{11}. Additionally, a minimum number of 8 passes is required to ensure an adequate initial mesh is generated and that the convergence doesn't preemptively exit.

For the coaxial unit ring, the convergence criteria must be a function of all of the diagonal entries of the S-Parameter matrix, i.e., the S11 values for all 9 propagating modes of the coaxial cavity. For the principal TEM mode, which is the mode that will be looked at for the reflected phase delay, the same convergence limit is set: a maximum change of no greater than 0.001 for the magnitude and 1 degree for the phase. For the other 8 modes the criteria require a maximum change of no greater than 0.01 for the magnitude and do not depend on phase.

For full convergence, 26 adaptive passes are needed for the coaxial unit ring, but in order to reduce simulation time, a maximum cut-off of 24 passes was used. This corresponds to a delta phase convergence of 1.28° instead of the desired 1°. Table #1 compares the performance of the unit cell and unit ring approaches. The unit ring results could be improved by allowing the adaptive process to go to 26 passes to match the unit cell criteria.

D. The PEC control case

An additional model must be created that is identical to those previously discussed, but with the radiating element replaced with a PEC block. In this way, a perfectly linear reflected phase shift can be obtained to compare to the reflected phase shift of the radiating element. The total reflected phase plot – which can be thought of as a "backwards S" curve (see Fig. 3) – can be found from subtracting the reflected phase of the PEC control case from the reflected phase of the radiating element.

III. SIMULATION RESULTS

Table 1 summarizes the findings and Fig. 3 presents the reflected phase plot produced by the two approaches. As might be expected, the unit cell is a much more computationally efficient way of calculating the reflected phase of the radiating patch. One important observation to note is that as the ring number increases the b/a ratio (where a is the inner and b is the outer radius of the coaxial unit cell) approaches unity, the physical area of the ring increases, and the number of propagating modes will approach infinity. Thus, another important quality of the unit cell model is that it will involve the same number of propagating modes as its location changes and the design is much easier to simulate for large radial locations.

Table 1: Mesh information for the coaxial wedge unit cell and the coaxial unit ring approach (2nd ring)

Mesh Statistics	Coaxial Wedge Unit Cell	Coaxial Unit Ring
Total mesh size	67,091	427,054
Simulation time	20 min	36 hours
Number of adaptive passes	19	24
Number of modes	1	9
Operational freq. band (GHz) {±90°}	5.870-6.309	5.862-6.299
Resonant phase frequency (GHz)	6.114	6.106
Bandwidth	7.15%	7.15%
Phase difference at 6.11 GHz	4.46°	

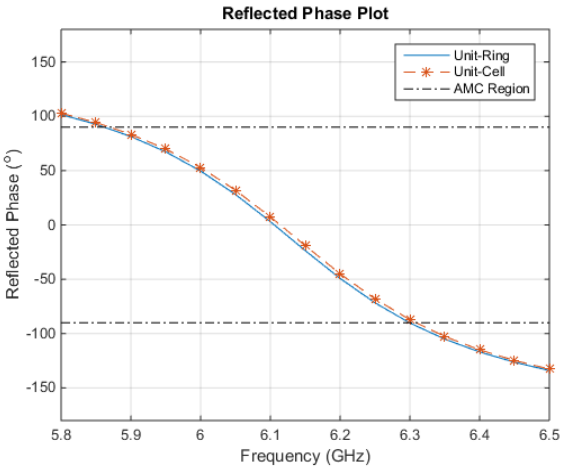

Fig. 3. Reflected phase curve for the two methods.

IV. REFLECTARRAY APPLICATION

As an example, consider a reflectarray for satellite communications in the commercial Ka-Band for an uplink frequency of 29 to 30 GHz and circular polarization. This antenna will be considered as a very small aperture terminal (VSAT) as it will have a total size of ~40cm. For this example, we design a reflectarray with a concentric ring topology. The design uses 47 rings, a spacing of 0.43 wavelengths between the rings, and 5α elements per ring where α is the integer ring index. The radius of the reflectarray is 20 wavelengths, for a total of 5,640 elements. The geometry of the reflectarray is shown in Fig. 4. This design has the minimum beamwidth required to meet the FCC 25.209 envelope, with a

gain of 42dB at 29.5GHz. A design with the unit cell parameters is presented in Table #2.

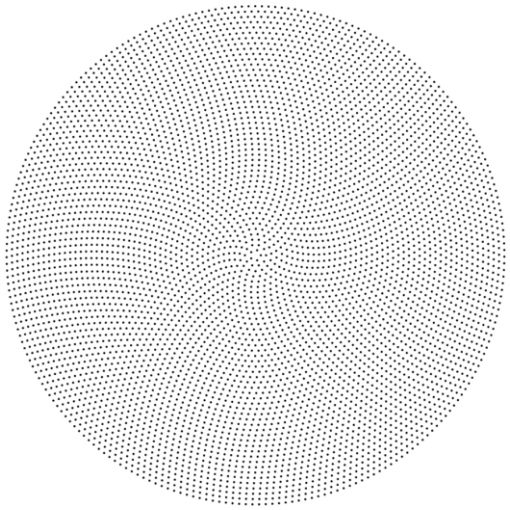

Fig. 4. Reflectarray geometry.

Table 2: Design table for the Ka-band unit cell

Design Table Ka-Band Unit cell	**Value**
Design frequency	29.5GHz
Substrate material	Roger RO3003
Substrate thickness	1.52mm
Radial (inner and outer) spacing	265μm
Angular spacing (cell, patch)	(36°, 28°)
Convergence criteria (mag, phase)	(0.001, 2.5°), 18 Passes
Resonant phase frequency (GHz)	29.54GHz
Bandwidth	1.42%

As discussed in the introduction, the phase shift ψ_i at an element must ensure that the phase delay at that element will produce a uniform reflected phase after path length delay effects are taken into account. This is equivalent to the constraint [36]:

$$k_0(R_i - \bar{r}_i \cdot \hat{r}_o) - \psi_i = 2\pi N, \quad (1)$$

where k_0 is the propagation constant, N is an integer, R_i is the distance to a patch, $\hat{r}_o$ is the unit vector of the reflected ray, and $\bar{r}_i$ represents the geometry of the array. A visual representation – from the geometry of this example – is depicted in Fig. 5.

In order to produce the phase shift required at an element by Fig. 5, the resonant phase as a function of patch size is needed. Notice that when the patch length is grown or shrunk, the resonant frequency will grow or shrink based on the trend depicted in Fig. 6, where patch length is defined as the radial length of the PEC patch within the unit cell. For frequency 29.5 GHz, and the set of resonant phase curves in Fig. 6, another backwards-S type curve can be produced for use as a design equation, as depicted in Fig. 7.

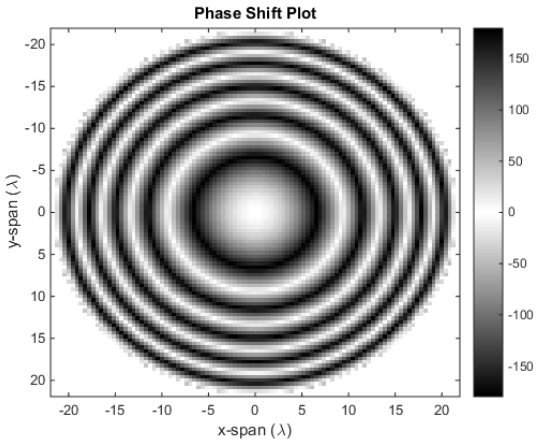

Fig. 5. Required element phase delay to produce a collimated beam using Equation #1.

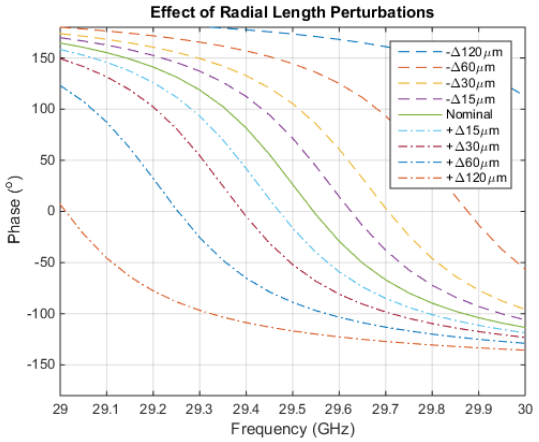

Fig. 6. Individual reflected phase plots for varying length elements.

After the resonant phase characteristics are determined and applied to the phase shift plot to produce a uniform reflected phase, the feed must be designed. The feed can be designed using simple reflector equations to find the optimal quality factor, where the optimal Q-factor is the maximum of the total aperture efficiency curve when combining spillover and illumination efficiencies. For this example, the F/D ratio was fixed at 1. The 3dB Beamwidth of the feed can be found using the following equations:

$$\theta_e = \tan^{-1}\left(\frac{1}{2F/D}\right) \rightarrow u = \cos(\theta_e), \quad (2)$$

$$\eta_{spillover} = 1 - u^{2(q+1)}, \quad (3)$$

$$\eta_{illumination} = \frac{4(q+1)(1-u^q)^2}{q^2 \eta_{spillover} \tan(\theta_e)^2}, \quad (4)$$

$$\eta_{total} = \eta_{spillover} \eta_{illumination}, \quad (5)$$

$$q_{max} = \max(\eta_{total}), \quad (6)$$

$$\Rightarrow BW_{3dB}(Feed) = 2\cos^{-1}\left(\exp\left\{\frac{\log\left(\frac{1}{2}\right)}{2q_{max}}\right\}\right), \quad (7)$$

$$with\ BW_{3dB}(Feed) \approx 30^\circ \left(for \frac{F}{D} = 1\right), \quad (8)$$

These equations produce the plots in Fig. 8, and the optimal Q-factor can be found as the maximum of the total aperture efficiency curve.

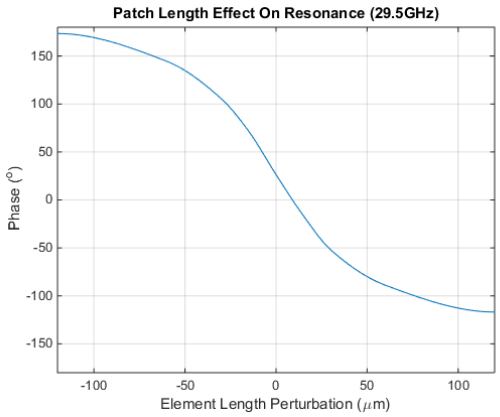

Fig. 7. Resonant phase plot for 12.4GHz versus element lengths.

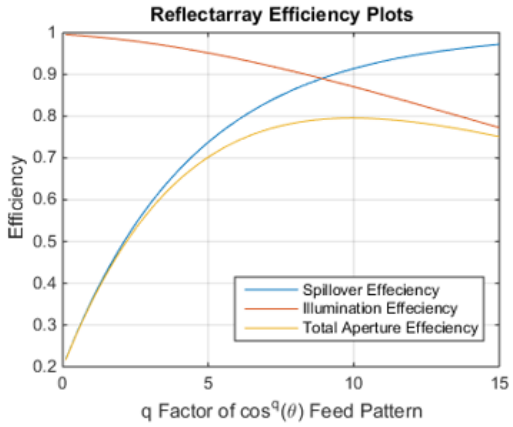

Fig. 8. Reflectarray efficiency plot.

Now that both the array and the feed are designed, the far-field pattern can be found using array theory with the feed and element patterns being applied as amplitude tapers (shown in Fig. 9). Assuming all elements are designed such that the phase delay requirement is met, the far-field plot will be that given in Fig. 10. The initial antenna pattern in Fig. 10 has a few sidelobes close to the main beam that violate regulatory requirements, but these can be mitigated using array optimization as described in [28].

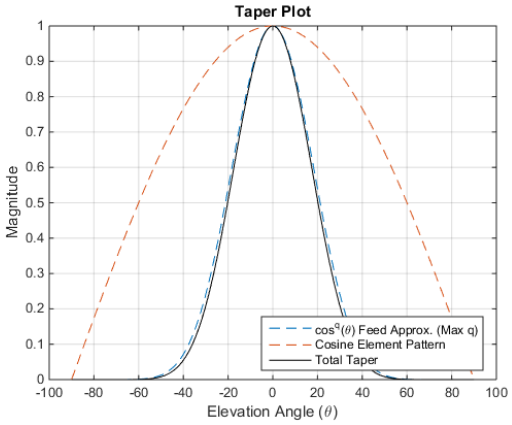

Fig. 9. Amplitude taper plot.

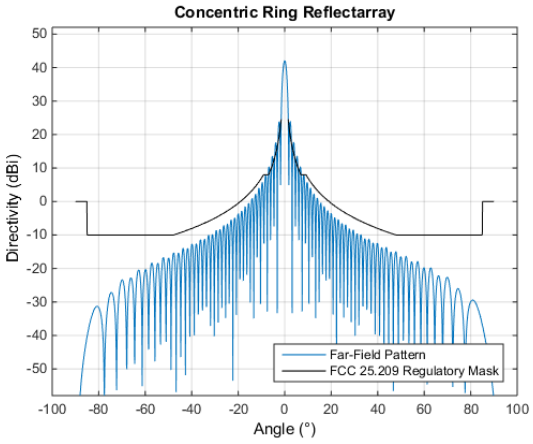

Fig. 10. Far-field pattern of the reflectarray antenna.

V. CONCLUSION

A method of designing a concentric ring reflectarray is presented. EM field simulation is used to determine the phase profiles of the unit cell. It is found that the coaxial wedge unit cell gives nearly identical results, in terms of bandwidth and resonant frequency of the reflected phase curve, compared to the coaxial unit ring. The coaxial wedge unit cell requires an order of magnitude smaller simulation time. A preliminary concentric-ring reflectarray design is presented.

REFERENCES

[1] D. Berry, R. Malech, and W. Kennedy, "The reflectarray antenna" *IEEE Transactions on Antennas and Propagation*, vol. 11, no. 6, pp. 645-651, Nov. 1963.

[2] H. R. Phelan, "Spiralphase reflectarray for multi-target radar," *Microwave Journal*, vol. 20, pp. 67-

73, July 1977.

[3] C. S. Malagisi, "Microstrip disc element reflect array," *Electronics and Aerospace Systems Convention*, pp. 186-192, Sept. 1978.

[4] J. P. Montgomery, "A microstrip reflectarray antenna element," *Antenna Applications Symposium*, University of Illinois, Sept. 1978.

[5] R. E. Munson and H. Haddad, "Microstrip reflectarray for satellite communication and RCS enhancement and reduction," U.S. Patent 4,684,952, Washington, D.C., Aug. 1987.

[6] J. Huang, "Microstrip reflectarray," *IEEE AP-S/URSI Symposium*, London, Canada, pp. 612-615, June 1991.

[7] T. A. Metzler, "Design and Analysis of a Microstrip Reflectarray," *Ph.D. Dissertation*, University of Massachusetts, Sept. 1992.

[8] Y. Zhang, K. L. Wu, C. Wu, and J. Litva, "Microstrip reflectarray: Full-wave analysis and design scheme," *IEEE AP-S/URSI Symposium*, Ann Arbor, Michigan, pp. 1386-1389, June 1993.

[9] D. M. Pozar and T. A. Metzler, "Analysis of a reflectarray antenna using microstrip patches of variable size," *Electronics Letters*, pp. 657-658, April 1993.

[10] R. D. Javor, X. D. Wu, and K. Chang, "Beam steering of a microstrip flat reflectarray antenna," *IEEE AP-S/URSI Symposium*, Seattle, Washington, pp. 956-959, June 1994.

[11] D. C. Chang and M. C. Huang, "Multiple polarization microstrip reflectarray antenna with high efficiency and low cross - polarization," *IEEE Trans. Antennas Propagat*., vol. 43, pp. 829-834, Aug. 1995.

[12] J. Huang, "Bandwidth study of microstrip reflectarray and a novel phased reflectarray concept," *IEEE AP - S/URSI Symposium*, Newport Beach, California, pp. 582-585, June, 1995.

[13] J. A. Encinar, "Design of a dual - frequency reflectarray using microstrip stacked patches of variable size," *Electronic Letters*, vol. 32, no. 12, pp. 1049-1050, June 1996.

[14] D. F. Sievenpiper, J. H. Schaffner, H. J. Song, R. Y. Loo, and G. Tangonan, "Two-dimensional beam steering using an electrically tunable impedance surface," *IEEE Transactions on Antennas and Propagation*, vol. 51, no. 10, pp. 2713-2722, Oct. 2003.

[15] S. V. Hum, M. Okoniewski, and R. J. Davies, "Modeling and design of electronically tunable reflectarrays," *IEEE Transactions on Antennas and Propagation*, vol. 55, no. 8, pp. 2200-2210, Aug. 2007.

[16] S. Xu, Y. Rahmat-Samii, and W. A. Imbriale, "Subreflectarrays for reflector surface distortion compensation," *IEEE Transactions on Antennas and Propagation*, vol. 57, no. 2, pp. 364-372, Feb. 2009.

[17] D. M. Pozar, S. D. Targonski, and H. D. Syrigos, "Design of millimeter wave microstrip reflect-arrays," *IEEE Transactions on Antennas and Propagation*, vol. 45, no. 2, pp. 287-296, Feb 1997.

[18] J. Huang and J. Encinar, *Reflectarray Antennas*. New York, United States: Wiley-IEEE Press, 2008.

[19] P. Hannan and M. Balfour, "Simulation of a phased-array antenna in waveguide," *IEEE Transactions on Antennas and Propagation*, vol. 13, no. 3, pp. 342-353, May 1965.

[20] W. L. Barrow and W. W. Mieher, "Natural oscillations of electrical cavity resonators," *Proceedings of the IRE*, vol. 28, no. 4, pp. 184-191, Apr. 1940.

[21] R. A. Kirkman and M. Kline, "The transverse electric modes in coaxial cavities," *Proceedings of the IRE*, vol. 34, no. 1, pp. 14p-17p, Jan. 1946.

[22] J. Sarrazin, A. C. Lepage, and X. Begaud, "Circular high-impedance surfaces characterization," *IEEE Antennas and Wireless Propagation Letters*, vol. 11, no., pp. 260-263, 2012.

[23] A. C. Durgun, C. A. Balanis, and C. R. Birtcher, "Reflection phase characterization of curved high impedance surfaces," *IEEE Transactions on Antennas and Propagation*, vol. 61, no. 12, pp. 6030-6038, Dec. 2013.

[24] M. A. Amiri, C. A. Balanis, and C. R. Birtcher, "Analysis, design, and measurements of circularly symmetric high-impedance surfaces for loop antenna applications," *IEEE Transactions on Antennas and Propagation*, vol. 64, no. 2, pp. 618-629, Feb. 2016.

[25] A. F. Peterson, S. L. Ray, and R. Mittra, *Computational Methods for Electromagnetics*. New York: IEEE Press, 1998.

[26] W. L. Stutzman and G. A. Thiele, *Antenna Theory and Design*. 3rd ed., New York: John Wiley & Sons, 2013.

[27] C. A. Balanis, Antenna *Theory: Analysis and Design*. 3rd ed., New York: John Wiley & Sons, 2005.

[28] R. L. Haupt, "Optimized element spacing for low sidelobe concentric ring arrays," *IEEE Transactions on Antennas and Propagation*, vol. 56, no. 1, pp. 266-268, Jan. 2008.

[29] Y. Rahmat-Samii and A. N. Tulintseff, "Diffraction analysis of frequency selective reflector antennas," *IEEE Transactions on Antennas and Propagation*, vol. 41, no. 4, pp. 476-487, Apr. 1993.

[30] L. A. Costa, O. M. d. C. Pereira-Filho, and F. J. S. Moreira, "Quasi-trapezoidal microstrip spherical patches and arrays," *IET Microwaves, Antennas & Propagation*, vol. 10, no. 1, pp. 53-60, Jan. 9, 2016.

[31] D. J. Gregoire, "3-D conformal metasurfaces,"

IEEE Antennas and Wireless Propagation Letters, vol. 12, pp. 233-236, 2013.

[32] G. Tiberi, S. Bertini, A. Monorchio, G. Mazzarella, and G. Montisci, "A spectral rotation approach for the efficient calculation of the mutual coupling between rectangular apertures," *IEEE Antennas and Wireless Propagation Letters*, vol. 10, pp. 131-134, 2011.

[33] R. F. Harrington, *Cylindrical Wave Functions, Time-Harmonic Electromagnetic Fields*. Wiley-IEEE Press, 2001.

Joshua S. Roper received two B.S. degrees in Electrical engineering and Physics from Georgia Southern University in 2016 and an M.S. degree in Electrical and Computer Engineering from the Georgia Institute of Technology in 2017. He is currently working towards his Ph.D. degree in Electrical and Computer Engineering at the Georgia Institute of Technology. Since January 2018, he has been a member of Technical Staff at Viasat Inc., where his work focuses on electromagnetics for satellite communication applications.

Andrew F. Peterson received the B.S., M.S., and Ph.D. degrees in Electrical Engineering from the University of Illinois, Urbana-Champaign in 1982, 1983, and 1986 respectively. Since 1989, he has been a member of the faculty of the School of Electrical and Computer Engineering at the Georgia Institute of Technology, where he is now a full Professor. Within ACES, he has served at various times as a member of the Board of Directors, the Finance Committee Chair, the Publications Committee Chair, and the President. He also served as a Technical Co-chair for the 25th Annual Review of Progress in Applied Computational Electromagnetics (ACES 2009). He was elevated to ACES Fellow in 2008.

APPENDIX I. ANALYTICAL MODE PREDICTION

Cylindrical waveguide geometries have a wave function (the solution to the Helmholtz equation) of the form:

$$\psi = B_n(k_\rho \rho) h(n\phi) e^{\pm j k_z z}, \tag{9}$$

where $B_n(k_\rho\rho) \sim J_n(k_\rho\rho)$, $N_n(k_\rho\rho)$, $H_n^{(1)}(k_\rho\rho)$, $H_n^{(2)}(k_\rho\rho)$ and $h(n\phi) \sim \sin(n\phi), \cos(n\phi), e^{\pm jn\phi}$.

A. Coaxial waveguide modes

The modes are commonly known for the coaxial waveguide and were derived in the 1940s.

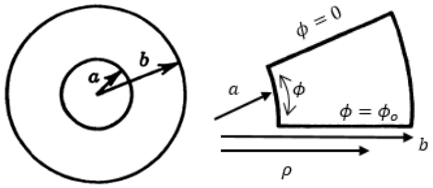

Fig. 11. Cross section of the coaxial waveguide (Left) and coaxial wedge waveguide (Right).

For the coaxial waveguide depicted in Fig. 11, by setting the electric field to zero at ρ = a and b, the propagation constant can be derived from the roots k_ρ of the equation:

$$Y_n(ka)J_n(kb) - J_n(ka)Y_n(kb) = 0, \quad \text{for } n = 0,1,2,\ldots \tag{10}$$

Similarly, for TE modes:

$$Y'_n(ka)J'_n(kb) - J'_n(ka)Y'_n(kb) = 0, \quad \text{for } n = 0,1,2,\ldots \tag{11}$$

The coaxial wedge waveguide is similar to the coaxial waveguide, but there are additional boundary conditions on the angular PEC walls. These require the electric field at φ = 0 and φ_0 to vanish. From these boundary conditions, the propagation constants can be derived from the roots k_ρ of the equation:

$$Y_n(ka)J_n(kb) - J_n(ka)Y_n(kb) = 0, \quad \text{for } n = \frac{k\pi}{\phi_o} \text{ where } k = 1,2,3\ldots \tag{12}$$

Similarly, for TE modes:

$$Y'_n(ka)J'_n(kb) - J'_n(ka)Y'_n(kb) = 0, \quad \text{for } n = \frac{k\pi}{\phi_o} \text{ where } k = 0,1,2,3\ldots \tag{13}$$

Since n is larger in the coaxial wedge waveguide than in the coaxial waveguide, the coaxial wedge waveguide will have fewer modes depending on the value of ϕ_o. We see this in practice – as in Table 1. Additional details on cylindrical wave functions can be found in [33].